Electric Potential of Ions in Electrode Micropores Deduced from Calorimetry

Joren E. Vos,[1] Danny Inder Maur,[1] Hendrik P. Rodenburg,[1,2] Lennart van den Hoven,[1] Suzan E. Schoemaker,[2] Petra E. de Jongh,[2] and Ben H. Erné[1,*]

[1]*Van 't Hoff Laboratory for Physical and Colloid Chemistry, Debye Institute for Nanomaterials Science, Utrecht University, Padualaan 8, 3584 CH Utrecht, Netherlands*

[2]*Materials Chemistry and Catalysis, Debye Institute for Nanomaterials Science, Utrecht University, Universiteitsweg 99, 3584 CG Utrecht, Netherlands*

(Received 1 February 2022; revised 15 July 2022; accepted 30 September 2022; published 28 October 2022)

The internal energy of capacitive porous carbon electrodes was determined experimentally as a function of applied potential in aqueous salt solutions. Both the electrical work and produced heat were measured. The potential dependence of the internal energy is explained in terms of two contributions, namely the field energy of a dielectric layer of water molecules at the surface and the potential energy of ions in the pores. The average electric potential of the ions is deduced, and its dependence on the type of salt suggests that the hydration strength limits how closely ions can approach the surface.

DOI: 10.1103/PhysRevLett.129.186001

Introduction.—In porous electrodes, the interface between solid conductor and liquid-phase ions is at the pore walls. Charge separation between solid and liquid occurs within less than a nanometer, and consequently, electrodes that largely consist of micropores (1–2 nm in width) have a huge electrified surface area. With carbon material, it can exceed 1000 m^2 per gram of solid, which allows for energy storage at high density. Moreover, since the charging process is rapid and reversible, "electrical double layer capacitors" are suitable for automotive and consumer applications [1,2]. Microporous electrodes are also applied in "capacitive deionization" to produce drinking water by removing salt from brackish water [3–5]. Conversely, electrical energy can be harvested from the mixing of dilute and concentrated salt solutions using capacitive electrodes [6,7].

The capacitance of a porous electrode provides experimental information about the electrical double layer inside the pores. From measurements at different ion-to-pore size ratios, it is clear that pores too narrow to accommodate ions do not store charge [8,9]. Nevertheless, solvated ions can lose their solvation shells when they enter into micropores [10–13]. In the field of capacitive deionization, theoretical models typically interpret the measured capacitance in terms of a dielectric layer of water molecules adsorbed at the pore walls (the "Stern layer") and an adjacent diffuse ionic layer [14,15]. The uptake of salt by microporous electrodes has been explained on the basis of a modified Donnan equilibrium, assuming that all in-pore ions are at the same electric potential [16,17]. More detailed insights can be obtained from numerical simulations, for instance using density functional theory or molecular dynamics [18–20]. Calculations as a function of distance from a pore wall show different profiles of the electric field and concentrations of ions, depending on the distance between opposing walls [21–24].

In the present Letter, we propose an experimental thermodynamic approach to characterize the average electric potential of ions inside a microporous electrode. The electrode is alternatingly charged or discharged, and the associated changes in internal energy are calculated from the amount of electrical work performed on the electrode [23] and from the exchanged heat, measured via calorimetry [25–32]. The changes in internal energy are dominated by the field energy of the electrical double layer, whose contribution scales quadratically with applied potential. However, this contribution is smaller than expected from the capacitance. Our explanation is that changes in applied potential do not fall fully across the capacitive part of the electrical double layer. The average electric potential of the ions in the pores is changed as well. Moreover, the internal energy is also affected by the attraction of ions to the carbon surface.

Experimental.—Experiments were conducted on microporous carbon electrodes in aqueous salt solutions. The porous working electrode (WE) was connected to an Ag/AgCl reference electrode (RE) and a porous carbon counter electrode (CE); see Fig. 1. Heat from the WE was

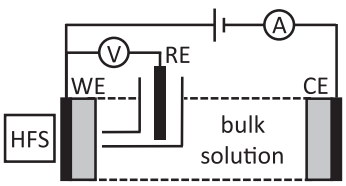

FIG. 1. Schematic of the experimental setup.

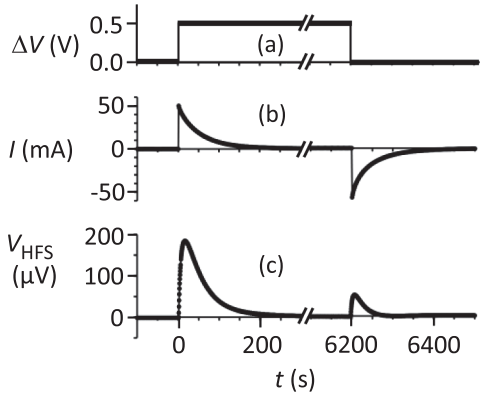

FIG. 2. Measurement of a charging-discharging cycle (1 M NaCl, 22 °C): time dependence of (a) applied potential referenced to open circuit potential after prolonged equilibration, (b) electric current, and (c) voltage of the heat flux sensor.

measured with a heat flux sensor (HFS). More details about the setup can be found in the Appendix.

The open circuit potential obtained after prolonged equilibration was chosen as the null point of applied potentials ΔV. Initially, at $\Delta V = 0$ V, the electric current I and HFS voltage V_{HFS} were close to zero. Then abruptly, a nonzero ΔV was applied, resulting in peaks of I and V_{HFS}; see Fig. 2. After 1 to 2 hours, $\Delta V = 0$ V was applied again. This charging-discharging cycle was repeated for $\Delta V = -0.5$ V to $+0.5$ V. The results were interpreted using the following model.

Theory.—The studied thermodynamic system consists essentially of four elements: (1) conductive carbon that is at the externally applied potential, (2) a dielectric layer of water molecules adsorbed at the pore walls, (3) ionic solution inside the pores, and (4) a nearby part of the bulk electrolyte solution reservoir, at constant electric potential V_{bulk}. Experiments start with prolonged equilibration at open circuit, until the carbon reaches an electric potential $V_{\mathrm{OCP,eq}}$. We neglect the presence of surface charge at open circuit, as was done in the interpretation of potential-dependent salt adsorption experiments on the same electrode material [17]. This implies that $V_{\mathrm{OCP,eq}} = V_{\mathrm{bulk}}$.

During charging, an electronic charge $+\Delta Q$ is added to carbon from the external circuit at potential $V_{\mathrm{OCP,eq}} + \Delta V$, and an ionic charge $-\Delta Q$ is added from bulk solution at potential $V_{\mathrm{OCP,eq}}$. The total electrical work on the system is therefore

$$w_{\mathrm{ch}} = \Delta Q \Delta V. \tag{1}$$

The measurements are essentially isothermal [33], and pressure-volume work is neglected. The energy change during charging is the sum of electrical work performed on the system and heat q_{ch} added to the system:

$$\Delta U_{\mathrm{ch}} = \Delta Q \Delta V + q_{\mathrm{ch}}. \tag{2}$$

During discharging, the electrical work on the system is

$$w_{\mathrm{dis}} = 0 \tag{3}$$

since ΔQ is removed from carbon at $\Delta V = 0$ V and ionic charge $-\Delta Q$ exits the system at $V_{\mathrm{OCP,eq}}$. The energy change now equals the discharging heat q_{dis}:

$$\Delta U_{\mathrm{dis}} = q_{\mathrm{dis}}. \tag{4}$$

For a full charging-discharging cycle, the total change in internal energy ΔU is zero, since the system begins and ends in the same state. Combining Eqs. (2) and (4) gives

$$q_{\mathrm{ch}} + q_{\mathrm{dis}} = -\Delta Q \Delta V. \tag{5}$$

This is the irreversible heat produced in resistive parts of the system. The HFS can be calibrated on this basis; see the Results section.

In order to interpret the experimental values of $\Delta U_{\mathrm{ch}} = -\Delta U_{\mathrm{dis}}$, it is assumed that the system's energy change consists of two contributions: the change ΔU_{w} in field energy of the dielectric water layer and the change ΔU_{ions} in potential energy of the ions in the pores:

$$\Delta U_{\mathrm{ch}} = \Delta U_{\mathrm{w}} + \Delta U_{\mathrm{ions}}. \tag{6}$$

Similarly, the change ΔV in applied potential consists of a change ΔV_{w} in voltage across the dielectric water layer and a change ΔV_{ions} in the average electric potential of the ionic solution inside the pores:

$$\Delta V = \Delta V_{\mathrm{w}} + \Delta V_{\mathrm{ions}}. \tag{7}$$

It is assumed that ΔV_{ions} is a fraction f of the change in applied potential:

$$\Delta V_{\mathrm{ions}} = f \Delta V. \tag{8}$$

The associated change in voltage across the dielectric water layer is given by

$$\Delta V_{\mathrm{w}} = (1 - f) \Delta V. \tag{9}$$

In our experiments, the measured capacitance C of the electrode is approximately constant:

$$\Delta Q = C \Delta V. \tag{10}$$

The combination of Eqs. (9) and (10) indicates that the capacitance of the dielectric water layer is given by

$$C_{\mathrm{w}} = C/(1 - f). \tag{11}$$

Consequently, the change in field energy during charging is given by

$$\Delta U_{\mathrm{w}} = \int_0^{(1-f)\Delta V} V C_{\mathrm{w}} dV = \frac{1}{2}(1-f)C(\Delta V)^2. \quad (12)$$

The energy change of the ionic solution is assumed to consist of two contributions: the electrical work to bring the countercharge $-C\Delta V$ to the in-pore potential $f\Delta V$, and an energy change $C\Delta V\Delta V_{\mathrm{att}}$ resulting from an attraction between the ions and carbon surface:

$$\Delta U_{\mathrm{ions}} = -fC(\Delta V)^2 + C\Delta V\Delta V_{\mathrm{att}}. \quad (13)$$

ΔV_{att} has units of V and represents a change in potential energy per elementary charge. The total energy change follows from Eqs. (6), (12), and (13):

$$\Delta U_{\mathrm{ch}} = \left[\frac{1}{2} - \frac{3}{2}f\right] C(\Delta V)^2 + C\Delta V\Delta V_{\mathrm{att}}. \quad (14)$$

Using Eqs. (2), (5), and (14), expressions for the heats of charging and discharging are found:

$$q_{\mathrm{ch}} = \left[-\frac{1}{2} - \frac{3}{2}f\right] C(\Delta V)^2 + C\Delta V\Delta V_{\mathrm{att}} \quad (15)$$

$$q_{\mathrm{dis}} = \left[-\frac{1}{2} + \frac{3}{2}f\right] C(\Delta V)^2 - C\Delta V\Delta V_{\mathrm{att}}. \quad (16)$$

When it is assumed that the irreversible heat q_{irr} is approximately the same upon charging and discharging [33], it is given by

$$q_{\mathrm{irr}} \cong \frac{q_{\mathrm{ch}} + q_{\mathrm{dis}}}{2} = -\frac{1}{2}C(\Delta V)^2 \quad (17)$$

and the reversible heat q_{rev} is given by

$$q_{\mathrm{rev}} \cong \frac{q_{\mathrm{ch}} - q_{\mathrm{dis}}}{2} = -\frac{3}{2}fC(\Delta V)^2 + C\Delta V\Delta V_{\mathrm{att}}. \quad (18)$$

Results.—Analysis of the experimental data started by integrating the current peaks, to obtain the change in equilibrium charge ΔQ; see Fig. 3(a). The measured charge was linear with applied potential and opposite during charging (ΔQ_{ch}) and discharging (ΔQ_{dis}). Capacitance was slightly higher in the cathodic range ($\Delta V < 0$) than in the anodic range ($\Delta V > 0$); see Table I.

Integration of a peak of the HFS voltage yielded the heat in HFS units (Vs), different upon charging (q_{ch}) or discharging (q_{dis}); see Fig. 3(b). As expected from Eq. (5), the integral of the two HFS voltage peaks was proportional to $-\Delta Q\Delta V$; see Fig. 3(d). The same proportionality constant in units of J/(Vs) was used to convert the separate heats of charging and discharging into energy

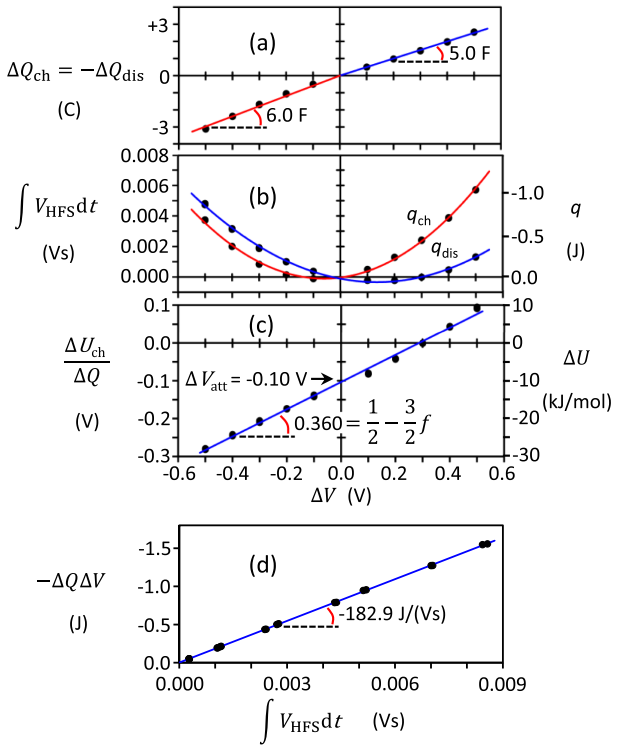

FIG. 3. Data analysis approach, illustrated for 1 M NaCl at 22 °C: (a) Potential dependence of equilibrium charge. (b) Potential dependence of the heats of charging and discharging, in sensor units (left y axis) and energy units (right y axis). (c) Potential dependence of the charging energy [see Eq. (19)]; the right y axis gives charging energy in kJ/mol. (d) Irreversible heat $-\Delta Q\Delta V$ versus integrated HFS signal for a full charging-discharging cycle; see Eq. (5).

units; see Fig. 3(b). This assumed that the HFS had the same sensitivity to reversible heat produced by the porous network and to Joule heat, used for the calibration. This assumption was not necessarily correct, for instance since part of the Joule heat was produced farther away from the HFS than the reversible heat. Some Joule heat came from a silver epoxy glue contact near the edge of the current collector. Some Joule heat was also generated by electric current through the electrolyte solution between the reference electrode and the WE; this heat was concentration- and salt-dependent, due to differences in electrical conductivity [36]. The HFS was probably the most sensitive to heat generated in the porous network, close to and centered with respect to the HFS. Since reversible heat scales linearly with f and ΔV_{att} [see Eq. (18)], an overestimation of the reversible heat by 33% (in an extreme scenario [36]) would also overestimate f and ΔV_{att} by 33%.

The same absolute ΔU was obtained via Eqs. (2) and (4). In kJ/mol, the results were comparable for different salt solutions. In all cases, a plot of $\Delta U/\Delta Q$ versus ΔV as in Fig. 3(c) gave a straight line with a negative y intercept, as shown in the Supplemental Material [37]. Table I shows the values of constants f and ΔV_{att} from the fitting of the

TABLE I. Measured cathodic and anodic capacitances, and internal energy parameters f and ΔV_{att} from Eq. (14), for different aqueous salt solutions at 22 °C. Results at 1 M are given in order of increasing cationic hydration strength, as indicated by hydration enthalpy ΔH_{hyd} and hydration numbers from electrostatic modeling (N_{mod}) and electrochemical quartz crystal microbalance measurements (N_{EQCM}). For chloride, $-\Delta H_{hyd} = 365$ kJ/mol [34], $N_{mod} = 2.0$ [34], and $N_{EQCM} = 0.6$ [35].

Salt solution	$C_{cathodic}$ (F) ±0.2	C_{anodic} (F) ±0.2	f ±0.010	ΔV_{att} (V) ±0.020	Cation	$-\Delta H_{hyd}$ [34] (kJ/mol)	N_{mod} [34]	N_{EQCM} [35]
1 M CsCl	6.1	5.1	0.109	−0.092	Cs^+	280	2.1	0.5
1 M RbCl	5.9	5.1	0.099	−0.095	Rb^+	305	2.4	···
1 M KCl	5.9	5.0	0.101	−0.107	K^+	330	2.6	1.3
1 M NaCl	6.0	5.0	0.093	−0.103	Na^+	415	3.5	2.2
1 M LiCl	6.1	5.0	0.079	−0.125	Li^+	530	5.2	2.6
1 M $CaCl_2$	6.9	6.1	0.064	−0.155	Ca^{2+}	1600	7.2	3.7
1 M $MgCl_2$	7.1	5.3	0.059	−0.122	Mg^{2+}	1945	10.0	5.8
1 M $LaCl_3$	7.0	6.1	0.029	−0.148	La^{3+}	3310	10.3	···
0.1 M NaCl	5.3	4.8	0.119	−0.078				
5 M NaCl	6.7	5.7	0.081	−0.125				

results obtained at 22 °C to the following equation, obtained by dividing the terms in Eq. (14) by $\Delta Q = C\Delta V$:

$$\frac{\Delta U_{ch}}{\Delta Q} = \left[\frac{1}{2} - \frac{3}{2}f\right]\Delta V + \Delta V_{att}. \tag{19}$$

Temperature-dependent measurements with 1 M NaCl indicated that the absolute values of f and ΔV_{att} increased with temperature [37]. For all salts, the largest ΔU was measured at $\Delta V = -0.5$ V, ranging from −25 kJ/mol (CsCl) to −40 kJ/mol ($LaCl_3$). This is much less than the full hydration enthalpies of the ions [34], which range from −280 kJ/mol for Cs^+ to −3310 kJ/mol for La^{3+}; see Table I. This suggests that dehydration of ions as they entered into micropores was not a strong effect in our experiments.

Discussion.—To compare the experimental results to theoretical models of the electrical double layer, one approach is to focus on the reversible heat. In Ref. [33], it was identified as the entropic contribution to the grand potential, in agreement with Overbeek [48]. Glatzel *et al.* [49] supported this identification using density functional theory and calculated the negative ratio of reversible heat q_{rev} and electrical work w_{el}. For our experiments, Eq. (18) and $w_{el} = \frac{1}{2}C\Delta V^2$ indicate that this ratio is given by

$$-q_{rev}/w_{el} = +3f - 2\Delta V_{att}/\Delta V. \tag{20}$$

One of the conclusions in Ref. [49] is that steric ion interactions play a key role in determining the $-q_{rev}/w_{el}$ ratio. Ion-wall interactions were not taken into account in Ref. [49], corresponding to the case where $\Delta V_{att} = 0$ V. Larger hydrated ions lead to a smaller $-q_{rev}/w_{el}$ ratio, in line with the small values of f that we find for solutions with Mg^{2+}, Ca^{2+}, and La^{3+}, our most strongly hydrated ions. Theory predicts that the $-q_{rev}/w_{el}$ ratio becomes smaller at increasing ionic strength [49], in line with the relatively small values of f that we find in 5 M NaCl and 1 M $LaCl_3$, although theory overestimates the measured effects. One source of discrepancy is uncertainty about the dielectric constant of water inside micropores, expected to be much closer to that of ice than to that of liquid water [17,50]. A calculation [37] shows that our electrodes have the capacitance of a parallel plate capacitor with the thickness of a water molecule and a dielectric constant of 2.1, the experimental value for water between capacitor plates 1 nm apart [50]. Another source of discrepancy is the possibly higher sensitivity of the HFS to reversible heat than to Joule heat, an effect for which no corrections were made in our data analysis.

Our alternative approach to interpret the data focuses on the change in internal energy. The parameter f describes which part of a change in applied potential is felt on average by ions in the pores. One theory that gives a constant value of the electric potential in micropores is the modified Donnan theory [17], but it is not applicable here, since most of our experiments were at high ionic strength (≥ 1 M), where diffuse layer overlap is negligible. At high ionic strengths, theoretical calculations predict that much of the net ionic charge is close to the surface [21,22,51,52]. In our measurements, the weakness of the measured heat effects and the similar capacitances found with different salts suggest that steric hindrance is not a strong limiting factor for the entry of ions into the micropores. The ionic core diameters range from 0.14 nm (Li^+) to 0.36 nm (Cl^-) [34], the Stokes diameters from 0.24 nm (Cs^+) to 0.48 nm (Li^+) [53–55], and the hydrated ion diameters from electrostatic modeling from 0.42 nm (K^+) to 0.62 nm (La^{3+}) [34]. This remains smaller than the wall-to-wall distance of 0.9 nm, an average of local values [8,56]. Nevertheless, there is a trend between the value of f and the strength with which the ions are hydrated. Our least hydrated ions are Cl^-, Cs^+, Rb^+, K^+, and Na^+, whereas Li^+, Ca^{2+}, Mg^{2+}, and La^{3+} are more strongly hydrated, in

that order, as indicated by hydration enthalpies and hydration numbers from electrostatic modeling [34] and electrochemical quartz microbalance measurements [35]; see Table I. Our results agree with the view that weakly hydrated ions come relatively close to the pore walls, where the electric potential changes strongly with applied potential—resulting in relatively high values of f—and that strongly hydrated ions remain farther away from the pore walls due to steric hindrance, resulting in lower values of f. This does raise the question of why this trend is not only observed in the cathodic range, where the cations are the counterions, but also in the anodic range, where the counterions are chloride. Our explanation is that at 1 M salt concentration, the ionic strength is sufficiently high that "ion swapping" occurs [8]. Both types of ions are present in the pores across the entire potential range, and a positive shift in applied potential causes an exchange of positive ions by negative ions.

The origin of the ion attraction parameter ΔV_{att} remains speculative. The typical value of -0.1 V corresponds to $-4k_BT$ per elementary charge. Direct evidence for the attraction of ions to the electrode surface was given by the detection of excess salt inside micropores in the absence of an externally applied potential [17,57], and this was ascribed to image charge attraction [17,58–60]. However, the resulting contribution to the potential energy would then probably depend on the applied potential [17], whereas in the fitting of our data, ΔV_{att} is a constant. An alternative is a more chemical explanation, for instance involving Van der Waals attraction [19,61]. In the present Letter, the ΔV_{att} parameter can be viewed as an empirical way to account for the asymmetry of measured heat versus applied potential. In most of our experiments, the reversible charging heat is clearly exothermic in the anodic range and endothermic in the cathodic range, an example of electrostatic cooling [62]. Although we ascribed the origin of the ΔV_{att} parameter to ion-carbon attraction, it cannot be ruled out that ΔV_{att} partly originates from the presence of net surface charge at open circuit. It is noted that the ΔV_{att} parameter could not be detected in earlier measurements of the total heat from the cathode and anode [33], since the $\pm\Delta Q\Delta V_{\mathrm{att}}$ contribution to the (dis)charging heat of the cathode canceled with the $\mp\,\Delta Q\Delta V_{\mathrm{att}}$ contribution to the (dis)charging heat of the anode; see Eqs. (15) and (16).

Conclusion.—The potential-dependent internal energy of porous carbon electrodes was determined experimentally. The precise scaling of the internal energy with applied potential was interpreted in terms of the average electric potential felt by ions inside the pores, which depends on the hydration strength of the ions. Moreover, a nonzero potential energy of the ions at open circuit was ascribed to a potential-independent attraction of the ions to the carbon surface. In the future, calorimetric measurements could be valuable to characterize the electrical double layer inside other types of porous electrodes, for instance supercapacitors. Also, numerical simulations using molecular dynamics or density functional theory could be performed to account for our experimental results. Moreover, further experimental information could be obtained about our experimental system, for instance by detecting in-pore ionic concentrations via *in situ* NMR spectroscopy.

Henkjan Siekman is thanked for making the electrochemical cell, Ties Bakker for preliminary measurements, and Bonny Kuipers, Dominique Thies-Weesie, and Alex van Silfhout for technical support. Maarten Biesheuvel is thanked for the carbon electrode material and for helpful discussions. Albert Philipse, Willem Kegel, and Andreas Härtel are thanked for helpful discussions as well. This publication is part of the project "Experimental Thermodynamics of Ion Confinement in Porous Electrodes" with Project No. 712.018.001 of the research program ECHO financed by the Dutch Research Council (NWO).

Appendix on experimental details.—Our experimental approach was inspired by Janssen *et al.* [33], with important differences. Rather than being measured from a complete electrochemical cell, heat was now detected from a single electrode; see Fig. 1. Furthermore, measurements were no longer in a two-electrode configuration, but three electrodes were used. A PARSTAT PMC-1000 potentiostat controlled the electric potential of the porous working electrode (WE) with respect to an Ag/AgCl/saturated KCl RE (Radiometer REF201), and the measured current flowed toward a CE.

Both WE and CE were porous carbon disks of the same material as in Ref. [33], with a diameter of 21 mm, a thickness of $\sim$0.25 mm, a mass of 63 mg, a specific surface area of 1400 $\mathrm{m^2/g}$, a porosity of 60%, and an average distance between opposing pore walls of $\sim$0.9 nm [37]. Each porous disk was fixed at the center to a nonporous carbon disk, using nonconductive glue, and electrical contact was realized by using a rubber O-ring and a flat Teflon ring (internal diameter: 18.5 mm) to press the porous-nonporous disk combination against a fixed nonporous carbon disk, connected at the back via silver epoxy glue to electrically insulated copper wire.

As in work by Munteshari *et al.* [30], heat from the WE was measured with a heat flux sensor (gSKIN® XP 26 9C, greenTEG AG, Switzerland). Its voltage was read using a Keithley 2182A Nanovoltmeter. The glass electrochemical cell was immersed in water in a box thermostated by a Julabo F25 refrigerated-heating circulator. Aqueous solutions of neutral pH were prepared from Milli-Q water and high purity salts [37] that are stable in the applied potential range [63]. More details about the setup can be found in Ref. [36].

A typical experiment started by equilibrating cell temperature for two days while monitoring the open circuit potential, V_{OCP}. It stabilized at an equilibrium value $V_{\mathrm{OCP,eq}}$

of about +0.2 V vs RE [37]. Subsequently applied potentials V_{applied} were referred to $V_{\text{OCP,eq}}$ by giving values of $\Delta V = V_{\text{applied}} - V_{\text{OCP,eq}}$. Before the start of charging-discharging experiments, $\Delta V = 0$ V was applied, allowing ≥ 1 hour for the current to become minimal ($< 20\ \mu$A).

*Corresponding author.
B.H.Erne@uu.nl

[1] P. Simon and Y. Gogotsi, Perspectives for electrochemical capacitors and related devices, Nat. Mater. **19**, 1151 (2020).
[2] Y. Wang, Y. Song, and Y. Xia, Electrochemical capacitors: Mechanism, materials, systems, characterization and applications, Chem. Soc. Rev. **45**, 5925 (2016).
[3] S. Porada, R. Zhao, A. Van Der Wal, V. Presser, and P. M. Biesheuvel, Review on the science and technology of water desalination by capacitive deionization, Prog. Mater. Sci. **58**, 1388 (2013).
[4] M. E. Suss, S. Porada, X. Sun, P. M. Biesheuvel, J. Yoon, and V. Presser, Water desalination via capacitive deionization: What is it and what can we expect from it?, Energy Environ. Sci. **8**, 2296 (2015).
[5] L. Wang, Y. Zhang, K. Moh, and V. Presser, From capacitive deionization to desalination batteries and desalination fuel cells, Curr. Opin. Electrochem. **29**, 100758 (2021).
[6] D. Brogioli, Extracting Renewable Energy from a Salinity Difference Using a Capacitor, Phys. Rev. Lett. **103**, 058501 (2009).
[7] M. L. Jiménez, M. M. Fernández, S. Ahualli, G. Iglesias, and A. V. Delgado, Predictions of the maximum energy extracted from salinity exchange inside porous electrodes, J. Colloid Interface Sci. **402**, 340 (2013).
[8] A. C. Forse, C. Merlet, J. M. Griffin, and C. P. Grey, New perspectives on the charging mechanisms of supercapacitors, J. Am. Chem. Soc. **138**, 5731 (2016).
[9] C. Largeot, C. Portet, J. Chmiola, P. L. Taberna, Y. Gogotsi, and P. Simon, Relation between the ion size and pore size for an electric double-layer capacitor, J. Am. Chem. Soc. **130**, 2730 (2008).
[10] J. Chmiola, G. Yushin, Y. Gogotsi, C. Portet, P. Simon, and P. L. Taberna, Anomalous increase in carbon capacitance at pore sizes less than 1 nanometer, Science **313**, 1760 (2006).
[11] J. Chmiola, C. Largeot, P. L. Taberna, P. Simon, and Y. Gogotsi, Desolvation of ions in subnanometer pores and its effect on capacitance and double-layer theory, Angew. Chem., Int. Ed. **47**, 3392 (2008).
[12] Z. X. Luo, Y. Z. Xing, S. Liu, Y. C. Ling, A. Kleinhammes, and Y. Wu, Dehydration of ions in voltage-gated carbon nanopores observed by in situ NMR, J. Phys. Chem. Lett. **6**, 5022 (2015).
[13] C. Prehal, C. Koczwara, N. Jäckel, A. Schreiber, M. Burian, H. Amenitsch, M. A. Hartmann, V. Presser, and O. Paris, Quantification of ion confinement and desolvation in nanoporous carbon supercapacitors with modelling and *in situ* X-ray scattering, Nat. Energy **2**, 16215 (2017).
[14] D. Brogioli, R. Zhao, and P. M. Biesheuvel, A prototype cell for extracting energy from a water salinity difference by means of double layer expansion in nanoporous carbon electrodes, Energy Environ. Sci. **4**, 772 (2011).
[15] R. Zhao, P. M. Biesheuvel, H. Miedema, H. Bruning, and A. van der Wal, Charge efficiency: A functional tool to probe the double-layer structure inside of porous electrodes and application in the modeling of capacitive deionization, J. Phys. Chem. Lett. **1**, 205 (2010).
[16] S. Porada, L. Borchardt, M. Oschatz, M. Bryjak, J. S. Atchison, K. J. Keesman, S. Kaskel, P. M. Biesheuvel, and V. Presser, Direct prediction of the desalination performance of porous carbon electrodes for capacitive deionization, Energy Environ. Sci. **6**, 3700 (2013).
[17] P. M. Biesheuvel, S. Porada, M. Levi, and M. Z. Bazant, Attractive forces in microporous carbon electrodes for capacitive deionization, J. Solid State Electron. **18**, 1365 (2014).
[18] R. Burt, G. Birkett, and X. S. Zhao, A review of molecular modelling of electric double layer capacitors, Phys. Chem. Chem. Phys. **16**, 6519 (2014).
[19] T. Colla, M. Girotto, A. P. dos Santos, and Y. Levin, Charge neutrality breakdown in confined aqueous electrolytes: Theory and simulation, J. Chem. Phys. **145**, 094704 (2016).
[20] H. Tao, C. Lian, and H. Liu, Multiscale modeling of electrolytes in porous electrode: From equilibrium structure to non-equilibrium transport, Green Energy Environ. **5**, 303 (2020).
[21] G. Feng, R. Qiao, J. Huang, B. G. Sumpter, and V. Meunier, Ion distribution in electrified micropores and its role in the anomalous enhancement of capacitance, ACS Nano **4**, 2382 (2010).
[22] G. Feng and P. T. Cummings, Supercapacitor capacitance exhibits oscillatory behavior as a function of nanopore size, J. Phys. Chem. Lett. **2**, 2859 (2011).
[23] E. E. Fileti, Electric double layer formation and storing energy processes on graphene-based supercapacitors from electrical and thermodynamic perspectives, J. Mol. Model. **26**, 159 (2020).
[24] Z. Wang, D. L. Olmsted, M. Asta, and B. B. Laird, Electric potential calculation in molecular simulation of electric double layer capacitors, J. Phys. Condens. Matter **28**, 464006 (2016).
[25] J. M. Sherfey and A. Brenner, Electrochemical calorimetry, J. Electrochem. Soc. **105**, 665 (1958).
[26] R. Schuster, Electrochemical microcalorimetry at single electrodes, Curr. Opin. Electrochem. **1**, 88 (2017).
[27] J. Schiffer, D. Linzen, and D. U. Sauer, Heat generation in double layer capacitors, J. Power Sources **160**, 765 (2006).
[28] Y. Dandeville, P. Guillemet, Y. Scudeller, O. Crosnier, L. Athouel, and T. Brousse, Measuring time-dependent heat profiles of aqueous electrochemical capacitors under cycling, Thermochim. Acta **526**, 1 (2011).
[29] X. Zhang, W. Wang, J. Lu, L. Hua, and J. Heng, Reversible heat of electric double-layer capacitors during galvanostatic charging and discharging cycles, Thermochim. Acta **636**, 1 (2016).
[30] O. Munteshari, J. Lau, A. Krishnan, B. Dunn, and L. Pilon, Isothermal calorimeter for measurements of time-dependent heat generation rate in individual supercapacitor electrodes, J. Power Sources **374**, 257 (2018).
[31] A. Likitchatchawankun, G. Whang, J. Lau, O. Munteshari, B. Dunn, and L. Pilon, Effect of temperature on irreversible and reversible heat generation rates in ionic liquid-based

electric double layer capacitors, Electrochim. Acta **338**, 135802 (2020).
[32] A. Kundu, L. Pilon, and T. S. Fisher, A continuum model of heat transfer in electrical double-layer capacitors with porous electrodes under constant-current cycling, J. Power Sources **511**, 230404 (2021).
[33] M. Janssen, E. Griffioen, P. M. Biesheuvel, R. van Roij, and B. Erné, Coulometry and Calorimetry of Electric Double Layer Formation in Porous Electrodes, Phys. Rev. Lett. **119**, 166002 (2017).
[34] Y. Marcus, A simple empirical model describing the thermodynamics of hydration of ions of widely varying charges, sizes, and shapes, Biophys. Chem. **51**, 111 (1994).
[35] M. D. Levi, S. Sigalov, G. Salitra, R. Elazari, and D. Aurbach, Assessing the solvation numbers of electrolytic ions confined in carbon nanopores under dynamic charging conditions, J. Phys. Chem. Lett. **2**, 120 (2011).
[36] J. E. Vos, H. P. Rodenburg, D. Inder Maur, T. J. W. Bakker, H. Siekman, and B. H. Erné, Three-electrode cell calorimeter for electrical double layer capacitors, arXiv:2210.00980.
[37] See Supplemental Material at http://link.aps.org/supplemental/10.1103/PhysRevLett.129.186001 for provenance and purity of the salts, temperature-dependent measurements, characterization of the porous electrode material by nitrogen physisorption at 77 K, and an extended version of Table I, which includes Refs. [38–47].
[38] P. M. Biesheuvel, R. Zhao, S. Porada, and A. van der Wal, Theory of membrane capacitive deionization including the effect of the electrode pore space, J. Colloid Interface Sci. **360**, 239 (2011).
[39] S. Porada, M. Bryjak, der Wal, and P. M. Biesheuvel, Effect of electrode thickness variation on operation of capacitive deionization, Electrochim. Acta **75**, 148 (2012).
[40] R. Zhao, O. Satpradit, H. H. M. Rijnaarts, P. M. Biesheuvel, and A. Wal, Optimization of salt adsorption rate in membrane capacitive deionization, Water Res. **47**, 1941 (2013).
[41] R. Zhao, M. van Soestbergen, H. H. M. Rijnaarts, A. van der Wal, M. Z. Bazant, and P. M. Biesheuvel, Time-dependent ion selectivity in capacitive charging of porous electrodes, J. Colloid Interface Sci. **384**, 38 (2012).
[42] R. Zhao, P. M. Biesheuvel, and A. van der Wal, Energy consumption and constant current operation in membrane capacitive deionization, Energy Environ. Sci. **5**, 9520 (2012).
[43] R. Zhao, S. Porada, P. M. Biesheuvel, and A. van der Wal, Energy consumption in membrane capacitive deionization for different water recoveries and flow rates, and comparison with reverse osmosis, Desalination **330**, 35 (2013).
[44] M. H. Polley, W. D. Schaeffer, and W. R. Smith, Physical adsorption studies in carbon black technology, Can. J. Chem. **33**, 314 (1955).
[45] R. S. Mikhail, S. Brunauer, and E. E. Bodor, Investigations of a complete pore structure analysis: I. Analysis of micropores, J. Colloid Interface Sci. **26**, 45 (1968).
[46] E. P. Barrett, L. G. Joyner, and P. P. Halenda, The determination of pore volume and area distributions in porous substances. I. Computations from nitrogen isotherms, J. Am. Chem. Soc. **73**, 373 (1951).
[47] J. Lyklema, *Fundamentals of Interface and Colloid Science: Fundamentals*, Fundamentals of Interface & Co (Elsevier Science, London, 1991), p. 736.
[48] J. T. G. Overbeek, The role of energy and entropy in the electrical double layer, Colloids Surf. **51**, 61 (1990).
[49] F. Glatzel, M. Janssen, and A. Härtel, Reversible heat production during electric double layer buildup depends sensitively on the electrolyte and its reservoir, J. Chem. Phys. **154**, 064901 (2021).
[50] L. Fumagalli, A. Esfandiar, R. Fabregas, S. Hu, P. Ares, A. Janardanan, Q. Yang, B. Radha, T. Taniguchi, K. Watanabe, G. Gomila, K. S. Novoselov, and A. K. Geim, Anomalously low dielectric constant of confined water, Science **360**, 1339 (2018).
[51] A. Härtel, M. Janssen, S. Samin, and R. van Roij, Fundamental measure theory for the electric double layer: Implications for blue-energy harvesting and water desalination, J. Phys. Condens. Matter **27**, 194129 (2015).
[52] A. Härtel, S. Samin, and R. van Roij, Dense ionic fluids confined in planar capacitors: In- and out-of-plane structure from classical density functional theory, J. Phys. Condens. Matter **28**, 244007 (2016).
[53] M. J. Kadhim and M. I. Gamaj, Estimation of the diffusion coefficient and hydrodynamic radius (Stokes radius) for inorganic ions in solution depending on molar conductivity as electro-analytical technique-a review, J. Chem. Rev. **2**, 182 (2020).
[54] P. C. F. Pau, J. O. Berg, and W. G. McMillan, Application of Stokes' law to ions in aqueous solution, J. Phys. Chem. **94**, 2671 (1990).
[55] Y. Marcus, Are ionic Stokes radii of any use?, J. Solution Chem. **41**, 2082 (2012).
[56] P. J. F. Harris, Fullerene-like models for microporous carbon, J. Mater. Sci. **48**, 565 (2013).
[57] T. Kim, J. E. Dykstra, S. Porada, A. van der Wal, J. Yoon, and P. M. Biesheuvel, Enhanced charge efficiency and reduced energy use in capacitive deionization by increasing the discharge voltage, J. Colloid Interface Sci. **446**, 317 (2015).
[58] S. Kondrat and A. Kornyshev, Superionic state in double-layer capacitors with nanoporous electrodes, J. Phys. Condens. Matter **23**, 022201 (2011).
[59] S. Kondrat, N. Georgi, M. V. Fedorov, and A. A. Kornyshev, A superionic state in nano-porous double-layer capacitors: Insights from Monte Carlo simulations, Phys. Chem. Chem. Phys. **13**, 11359 (2011).
[60] B. Skinner, M. S. Loth, and B. I. Shklovskii, Capacitance of the Double Layer Formed at the Metal/Ionic-Conductor Interface: How Large Can It Be?, Phys. Rev. Lett. **104**, 128302 (2010).
[61] Z. X. Luo, Y. Z. Xing, Y. C. Ling, A. Kleinhammes, and Y. Wu, Electroneutrality breakdown and specific ion effects in nanoconfined aqueous electrolytes observed by NMR, Nat. Commun. **6**, 6358 (2015).
[62] S. Porada, H. V. M. Hamelers, and P. M. Biesheuvel, Electrostatic cooling at electrolyte-electrolyte junctions, Phys. Rev. Research **1**, 033195 (2019).
[63] M. Pourbaix, *Atlas of Electrochemical Equilibria in Aqueous* (National Association of Corrosion Engineers, Houston, 1974).